

Constitutive Properties of Hard-Alpha Titanium

K.S. CHAN, L. PEROCCHI, and G.R. LEVERANT

The flow and fracture behavior of hard-alpha Ti was studied as a function of nitrogen content, stress state, strain rate, and temperature. Hard-alpha Ti specimens with nitrogen contents ranging from 2 to 11.6 wt pct were fabricated by powder-metallurgy techniques. Stress-strain curves were obtained under various states of stress by performing uniaxial compression, indirection tension, indentation, and plane-strain compression tests at two strain rates. By varying the test technique and the specimen geometry, deformation and fracture in hard-alpha Ti was characterized for mean pressures as high as 6 times the flow stress. Most of these tests were conducted at 954 °C, but some were performed at 25 °C, 927 °C, and 982 °C. The experimental results indicated that, during compression testing at 927 °C to 982 °C, hard-alpha Ti exhibited substantial plastic deformation for nitrogen contents less than 4 wt pct, but showed brittle fracture with little plastic flow for nitrogen contents of 5.5 to 11.6 wt pct. Both the yield and fracture strengths increase with increasing nitrogen content and pressure, but decrease with increasing temperature. The yield strength increases with strain rate, while the fracture strength shows little or no rate sensitivity. The fracture strength in tension is substantially lower than that in compression. These observed deformation and fracture characteristics are explained on the basis of microcrack formation during inelastic deformation.

I. INTRODUCTION

PREMIUM-grade titanium alloys, formerly processed by double vacuum arc remelting (VAR) and now processed by triple VAR, are used for fan and compressor rotors and disks in aircraft jet engines. Occasional upsets during processing can result in the formation of nitrogen-rich alpha titanium (also referred to as hard-alpha in this article), which is brittle and often has microcracks and microvoids associated with it. The hard-alpha anomalies were measured to contain 3.5 to 14.8 wt pct N and up to 2.5 wt pct O.^[1] A chemical or compositional definition of hard-alpha does not exist, but it is generally accepted that hard-alpha contains at least a few weight percentages (*e.g.*, 3 to 4 wt pct) of nitrogen. The only defining characteristic of hard-alpha Ti is that it has a high hardness, which is influenced, in addition to N, by other interstitials and alloying elements also. Although rare, the hard-alpha anomalies have led to uncontained engine failures that resulted in fatal accidents such as the incident at Sioux City in 1989.

As a result of the accident at Sioux City, the Federal Aviation Administration (FAA) requested in 1991 that industry, through the Aerospace Industries Association (AIA), review available techniques to see whether a damage-tolerance approach could be introduced to produce a reduction in the rate of uncontained rotor events. The industry working group concluded that additional enhancements to the conventional rotor-life-management methodology could be established that would explicitly address the hard-alpha anomalous conditions. In response to the AIA recommendations, the FAA "Titanium Rotating-Component Review Team Report,"^[2] and the AGARD (Advisory Group for Aerospace Research and

Development),^[3] National Aeronautics and Space Administration,^[4] and United States Air Force^[5,6] experience and recommendations on damage-tolerance concepts and operational experience for gas turbine disk alloys, the FAA in 1995 funded an industrial team, which consists of Southwest Research Institute, Allied Signal (which is now Honeywell), Rolls-Royce Allison, General Electric (GE), and Pratt & Whitney, to develop a probabilistic-based, damage-tolerance design code to augment the current safe-life approach for life management of commercial aircraft gas turbine rotors/disks. The design code is not intended to replace existing design methods, but to provide an additional tool that the engine manufacturers can use for reliability assessment.

Under the sponsorship of the FAA, the industrial team has developed a probabilistic design methodology for treating hard-alpha defects in Ti rotors. A supplementary effort has involved the development of a microcode that is incorporated into a commercial finite-element forging code (DEFORM*) to allow tracking of the size, shape, and defor-

*DEFORM is a trademark of Scientific Forming Technologies, Columbus, OH.

mation histories of hard-alpha defects during forging of Ti alloys from ingot to rotor geometries. The development of the microcode required the constitutive properties of hard-alpha Ti as a function of nitrogen content, stress state, strain rate, and temperature. While there have been studies on the phase transformation,^[7] phase formation,^[8] processing route and microstructure,^[9] nondestructive inspection,^[9,10] and elastic properties,^[10] there is only limited information on the flow and fracture properties of hard-alpha Ti. The tensile fracture stress and the compressive flow stress were measured by Gigliotti for hard-alpha Ti samples having 2.5 and 3.54 wt pct N, respectively.^[11] To the authors' knowledge, no other published data on the flow and fracture properties are available. Because of this, this work was undertaken to develop an extensive constitutive-properties database for hard-alpha Ti.

The objective of this study was to establish the constitutive

K.S. CHAN, Institute Scientist, and G.R. LEVERANT, Program Director, are with the Southwest Research Institute, San Antonio, TX 78238-5166. L. PEROCCHI, Metallurgical Specialist, is with General Electric, CR&D Center, Schenectady, NY 12301.

Manuscript submitted January 13, 2000.

Table I. Nitrogen Contents and Young's Modulus of Synthetic Hard-Alpha Ti Specimens

Specimen	Nitrogen Content, Wt Pct	E , GPa (954 °C)
2N	2.0	41.4
4N	4.0	28.3
6N	5.5	51.0
9N	9.4	82.1
12N	11.6	124.8

properties of hard-alpha Ti for various nitrogen contents and stress states at several temperatures and two strain rates. The nitrogen contents investigated ranged from 2 to 11.6 wt pct N. Within this range of nitrogen contents, hard alpha is comprised of a single-phase α -Ti (hcp) with nitrogen in solid solution or a two-phase microstructure of α -Ti and Ti_2N ,^[9,12] depending on the nitrogen content and temperature. This range of nitrogen contents has been motivated by field data, which show that the nitrogen content in the diffusion-affected zone neighboring hard-alpha anomalies is about 2 wt pct, while the nitrogen content in the hard-alpha anomalies can be as high as 12 wt pct. The constitutive properties investigated in this study include the elastic modulus, yield stress, fracture strength, and flow stress of intact as well as damaged (fractured) materials. The development of constitutive relations between inelastic deformation and damage accumulation in hard-alpha is presented elsewhere.^[13]

II. EXPERIMENTAL PROCEDURES

A. Material

Synthetic hard-alpha ingots were prepared at the GE Corporate Research and Development Laboratory by melting a titanium metal sponge and TiN (titanium nitride) powder in a nonconsumable arc melter. Each of the ingots was melted 3 times. The ingot was turned over and weighed between each melt. Subsequently, the arc-melted hard-alpha alloy ingots were hot isostatically pressed (hipped) at 1200 °C under 207 MPa pressure for 4 hours to close any solidification porosity. The hipped ingot was then cut by electrodischarge machining (EDM) to yield two thin diametrical slices (each <2.5-mm thick). One slice was metallographically polished and examined to assure microstructural homogeneity. The other slice was cut (for example, with a diamond saw) into small pieces for chemical analysis. Oxygen analysis was carried out *via* a fusion technique (LECO*), while

*LECO is a trademark of LECO Corporation, St. Joseph, MI.

nitrogen analysis was performed *via* acid dissolution and titration (Kjeldahl). Analysis of the nitrogen content in weight percent, for the synthetic hard-alpha, is shown in Table I. All compositions reported in this article are in weight percent.

Test specimens were fabricated from the hipped ingots by EDM. The compression test specimens were 6.4-mm-diameter cylinders, 12.7 mm in height. The indirect-tension specimens were thin disks 9.5 mm in diameter and 3.2-mm thick. Both the indentation and plane-strain compression test specimens were 6.4 mm cubes. After EDM, the flat surfaces of the test specimens were ground. They were then etched in a solution of 60 vol pct distilled water, 30 vol pct nitric

acid, and 10 pct hydrofluoric acid to clean surfaces, followed by a rinse in propanol. All the specimens were tested in the as-received condition at SOUTHWEST RESEARCH INSTITUTE* after inspection for surface cracks.

*SOUTHWEST RESEARCH INSTITUTE is a trademark of Southwest Research Institute, San Antonio, TX.

The microstructures of hard-alpha with 2, 4, 5.5, and 11.6 wt pct N in the as-received condition are presented in Figures 1(a) through (d), respectively, which show two-phase microstructures containing alpha Ti and titanium nitride (Ti_2N). The amount of Ti_2N in the microstructure increases with increasing N content. According to a published phase diagram,^[12] the microstructure of hard alpha should be comprised of α -Ti and Ti_2N for 2 to 12 wt pct N at temperatures below 500 °C, which is qualitatively in agreement with the results shown in Figure 1. At the test temperatures (927 °C to 980 °C), hard-alpha specimens with 2 and 4 wt pct N are expected to be in the α -Ti phase field, while those with 5.5, 9.4, and 11.6 wt pct N are expected to be in the two-phase field of α -Ti and Ti_2N .^[12]

B. Constitutive Testing

The constitutive behavior of hard-alpha was characterized as a function of temperature, strain rate, nitrogen content, and stress state. The stress state was varied by employing different testing techniques and specimen geometries. As summarized in Figure 2, the constitutive tests include (1) uniaxial compression, (2) indirect tension (Brazilian test), (3) indentation, and (4) plane-strain compression. Indirect-tension tests were preferred over conventional tensile tests, because it is extremely difficult to fabricate tensile specimens of hard-alpha due to its brittleness. The procedures of the various constitutive tests are described subsequently.

1. Compression tests

Compression tests were conducted on cylindrical bars 6.4 mm in diameter and 12.7 mm in height. Testing was conducted in a servohydraulic testing machine equipped with an induction heating unit. To eliminate friction, boron nitride, a spray lubricant, was applied to the interface between the silicon carbide loading blocks and the test specimen. The test temperatures were 927 °C, 954 °C, and 982 °C, while the strain rates were 0.01 and 1 s⁻¹. The nitrogen contents of the test specimens were 2, 4, 5.5, 9.4, and 11.6 pct nitrogen by weight, as shown in Table I. All tests except those for the 2 pct N specimens were conducted under displacement-controlled conditions, because of little or no plastic flow in these materials. The 2 pct N specimens exhibited substantial plastic deformation, so testing was conducted under computer-controlled constant-strain-rate conditions. Load-displacement data were measured using a computer data acquisition system and were subsequently converted into stress-strain data.

2. Indirect-tension tests

The indirect-tension (Brazilian) tests were conducted by compressing circular thin disks on edge using the same experimental setup described earlier for the compression tests. The disk specimens were 3.2 mm in thickness and 9.5 mm in diameter. Small cracks were detected in some of the disk specimens prior to testing, and they were not used. Testing was performed on crack-free specimens of several

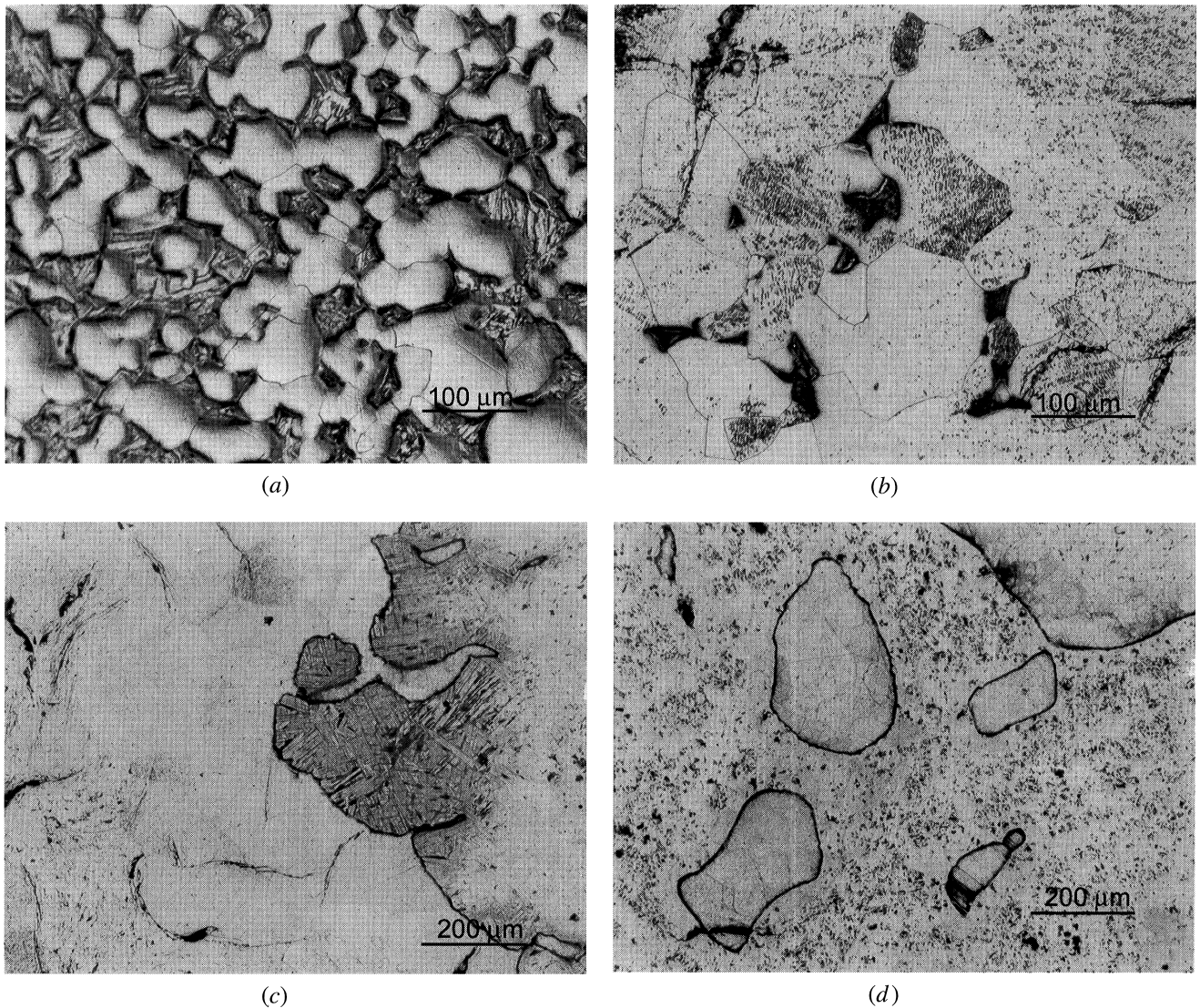


Fig. 1—Microstructures of hard-alpha in the as-received condition: (a) 2 wt pct N, (b) 4 wt pct N, (c) 5.5 wt pct N, and (d) 11.6 wt pct N.

nitrogen contents at 954 °C under a strain rate of 1 s^{-1} . One test was performed on a specimen (B6N-A) with a small crack oriented perpendicular to the compression axis. This small crack was closed during testing and did not affect the test result. For comparison, one test was also performed at a strain rate of 0.01 s^{-1} . Load-displacement curves were measured up to fracture, which occurred at the center of the specimens

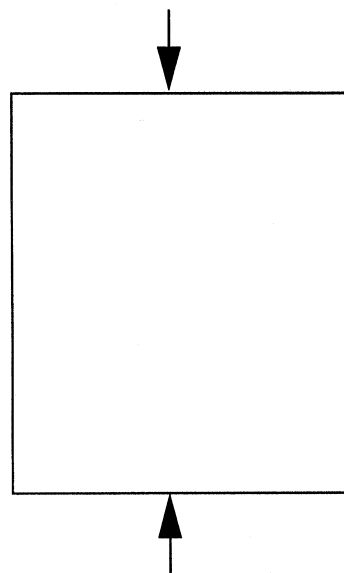
3. Indentation tests

Indentation tests were conducted on 6.44-mm cube specimens using a silicon carbide indenter and the same experimental setup used in the compression tests. The indenter was semispherical, with a 1.5-mm radius. Indentation tests were performed on specimens with five different nitrogen contents (2, 4, 5.5, 9.4, and 11.6 wt pct N). All tests were conducted at 954 °C under displacement-controlled conditions that corresponded to average strain rates of 1 and 0.01 s^{-1} . Load was measured as a function of indentation depth, and the test was terminated when a large load drop occurred or after the indentation depth exceeded a distance equal to the radius (1.5 mm) of the indenter. For the 2 pct N specimens, the indenter penetrated completely into the hard-alpha

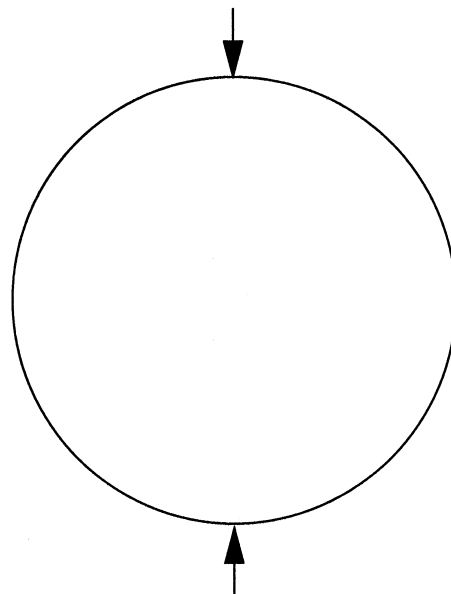
without causing cracking or fracture to the cube specimen. For higher nitrogen contents (>4 pct N), large cracks formed at the center of the specimen, causing it to fracture into several small pieces.

4. Plane-strain compression tests

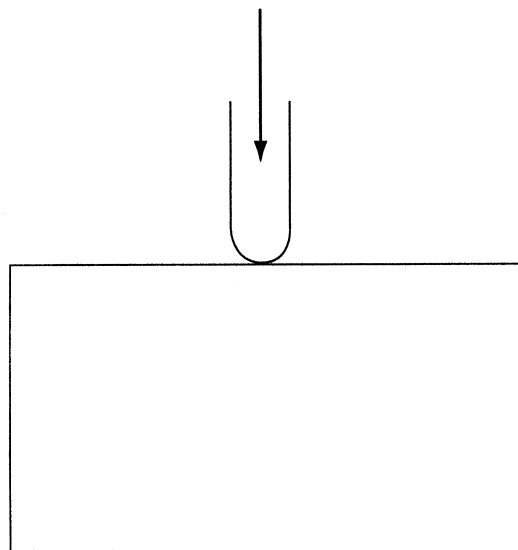
Plane-strain compression tests were conducted by compressing a flat plunger onto a 6.4-mm cube specimen in a die with a rectangular channel that prevented expansion of the specimen in the width direction. Schematics of the apparatus for the plane-strain compression tests are presented in Figure 3. Testing was performed at ambient temperature under constant displacement rates. The compliance of the servohydraulic test system was first obtained for the strain rates of interest, which were 0.01 and 1 s^{-1} . Plane-strain compression tests were then performed, and load-displacement data were measured. After testing, the compliance curve was then subtracted from the measured load-displacement data to obtain the actual load-displacement response of the test specimen. Plane-strain compression tests were performed for the 2N, 4N, 6N, and 9N specimens at 1 s^{-1} and for the 2N, 4N, 6N, 9N, and 12N specimens at 0.01 s^{-1} . All tests were conducted beyond the maximum load



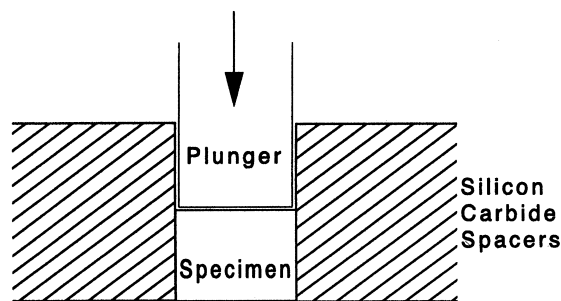
(a) Uniaxial compression of a cylindrical bar specimen



(b) Indirect tension by compressing a thin disk on edge



(c) Indentation of a cube specimen by an indenter with a semi-spherical tip



(d) Plane strain compression of a cube specimen

Fig. 2—(a) through (d) Testing techniques used to characterize the stress-strain behavior of hard- α under various stress states.

where the specimen fractured, and the straining was continued until the applied load dropped to almost zero. Postfracture straining was necessary to characterize the damage-induced softening response of the hard- α under constrained conditions.

C. Results

1. Compression tests

Table II summarizes the results of the compression tests. The table includes the test temperature, strain rate, yield stress, fracture stress, and mode of failure. The initial slope of the stress-strain curves for compression tests was used

to determine an approximate Young's modulus for hard- α . These results, summarized in Table I, show that the Young's modulus of hard- α increases with increasing nitrogen content. In uniaxial compression, hard- α Ti was ductile at 2 wt pct N, but fracture intervened during plastic deformation at 4 wt pct N. The measured flow stress and ultimate fracture strength were consistent with the GE data for 3.4 wt pct N,^[11] which are also shown in Table II. Hard- α Ti failed by fracture without appreciable plastic deformation, for nitrogen contents at or greater than 5.5 wt pct. The stress-strain curves of hard- α Ti, for compression at 954 °C under a strain rate of 1 s⁻¹, are presented in Figure 4, while those for a strain rate of 0.01 s⁻¹ are shown

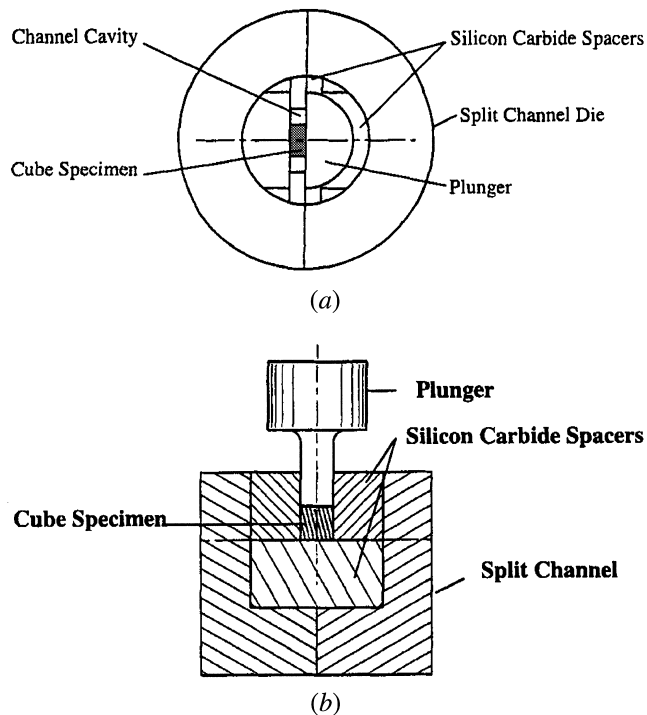


Fig. 3—Schematics of the plane strain compression test apparatus: (a) top view and (b) side view.

in Figure 5. Hard-alpha Ti with 11.6 wt pct N failed by fracture under compression at 927 °C, 954 °C, and 982 °C and a strain rate of 1 s^{-1} , as presented in Table II.

2. Indirect-tension (Brazilian) tests

Five Brazilian specimens were tested by edge compression of thin disks. Two of these specimens contained 2 wt pct N, which were very ductile and did not fail by fracture. As a result, the tensile fracture stress was not obtained for the 2 wt pct N material. The remaining three crack-free Brazilian specimens were tested, and they failed by elastic fracture, yielding valid values of the fracture stress. One specimen that contained a very small crack near the edge was also tested, with the known crack aligned normal to the applied compressive stress. A summary of the Brazilian tests is presented in Table II. Tensile-test results from GE Corporate Research and Development for hard-alpha with 2.5 wt pct N^[11] are also included in Table II.

The load-displacement curves for the indirect-tension tests of hard-alpha Ti are shown in Figure 6. The result for 2 wt pct N was that it was very ductile and did not fail by brittle fracture. All other specimens failed by brittle fracture when tested by indirect tension. For specimens that failed by brittle fracture, the elastic-stress analysis^[14] was used to analyze the data. According to this analysis, the tensile fracture stress at the center of a thin disk under edge compression is one-third of the peak compression stress applied at the edge. Using this method, the peak load at fracture was used to calculate the tensile fracture stress at the center of the disk, and the results are summarized in Table II. A comparison of the tensile fracture strength against those specimens in compression indicates that hard-alpha Ti fractured at a substantially lower stress in tension (35 to 72 MPa) than in compression (489 to 725 MPa).

3. Indentation tests

Indentation tests of hard-alpha Ti were performed as a function of nitrogen content at 954 °C for displacement rates of 0.254 and 25.4 mm/s, which corresponded to approximate, average strain rates of 0.01 and 1 s^{-1} , respectively. One test was also performed at 982 °C for hard-alpha Ti with 11.6 wt pct N. A summary of the indentation tests is presented in Table II together with the compression, Brazilian, and plane-strain compression tests.

Figure 7 shows a plot of the average pressure vs the average strain, for the indentation tests at 954 °C under a strain rate of 1 s^{-1} . Hard-alpha Ti with 2 wt pct N was ductile and exhibited plastic flow without fracture when tested by indentation. With 4 wt pct N, hard-alpha Ti exhibited plastic flow and localized fracture after yielding. For nitrogen contents >5.5 wt pct, hard-alpha Ti showed fracture with little plastic flow.

The indentation test results were analyzed using a method attributed to Tabor^[15] and Dieter.^[16] For a perfectly plastic material, the average pressure (P) for indentation by a spherical indenter under full plasticity conditions is related to the flow stress (Y_n) at a given strain, according to

$$Y_n = P/2.8 \quad [1]$$

and the corresponding strain is given by^[15,16]

$$\varepsilon = 0.2(d/D) \quad [2]$$

where d is the diameter of the indentation and D is the diameter of the indenter. Equations [1] and [2] were used to obtain the yield and fracture stresses and the average true strain and strain rate of hard-alpha Ti during indentation, respectively, assuming that constrained yielding occurred under the indenter during indentation of both low- and high-nitrogen materials. The diameter of the indentation (d) was approximated by the penetration depth or displacement. These assumptions were justified and supported by the plane-strain test results, to be discussed in the next section. A summary of the yield and fracture stresses for the indentation tests is presented in Table II, together with the compression and Brazilian test results.

4. Plane-strain compression tests

Plane-strain compression tests were performed at ambient temperature by compressing the test specimen in the channel die beyond the maximum load, to characterize the softening response due to damage and microcracking. Ambient-temperature tests were used because of the complexities of high-temperature testing. In addition, the plane-strain tests were intended to characterize the fracture stresses of hard-alpha with a high nitrogen content as a function of strain beyond the maximum load. Since the hard-alpha specimens with high nitrogen contents (>5.5 wt pct) failed by brittle fracture in compression at 927 °C to 982 °C, the room-temperature tests were considered adequate for characterizing the fracture-stress values at various levels of strain beyond the maximum load. As it turned out, the fracture stresses measured at the peak load were found to be insensitive to the test temperature. Engineering stress-strain curves for hard-alpha Ti are shown in Figures 8 and 9 for strain rates of 0.01 and 1 s^{-1} , respectively. Engineering stress-strain data for the 2N material are not shown in Figures 8 and 9, because the material did not fracture when loaded to the maximum load capacity of the test machine. The stress-strain curves of the

Table II. A Summary of Yield Stress (σ_y) and Fracture Stress (σ_f) of Hard-Alpha Ti Tested In Compression, Indirect Tension, Indentation, and Plane Strain Compression

Specimen	T, °C	N, Wt Pct	Strain Rate, s ⁻¹	σ_y , MPa	σ_f , MPa	Type	Comment
2N-A	954	2	1	207	>300	C	yielding, no fracture
4N-A	954	2	1	469	489	C	yielding, no fracture
6N-A	954	5.5	1	—	555	C	fracture, no yielding
9N-A	954	9.4	1	—	725	C	fracture, no yielding
12N-A	954	11.6	1	—	661	C	fracture, no yielding
GE (3.4 wt pct N)	954	3.4	1	346	432	C	yielding, GE data ^[11]
4N-B	954	4	0.01	230	320	C	yielding/fracture
9N-B	954	9.4	0.01	—	696	C	fracture, no yielding
12N-C	954	11.6	0.01	—	786	C	fracture, no yielding
12N-D	927	11.6	1	—	812	C	fracture, no yielding
12N-E	982	11.6	1	—	611	C	fracture, no yielding
B2N-A	954	2	1	—	—	B	yielding, no fracture
B4N-A	954	4	1	—	35	B	fracture, no yielding
B4N-B	954	4	0.01	—	31	B	fracture, no yielding
B6N-A	954	5.5	1	—	35	B	fracture, no yielding
B9N	954	9.4	1	—	49	B	fracture, no yielding
GE (2.54 wt pct N)	954	2.54	—	43	72	T	yielding/fracture, GE data ^[11]
S2N-1	954	2	1	462	—	I	yielding
S4N-2	954	4	1	874	874	I	yielding/fracture
S6N-1	954	5.5	1	—	1074*	I	fracture
S9N-1	954	9.4	1	—	1611*	I	fracture
S12N-1	954	11.6	1	—	1425*	I	fracture
S12N-4	954	11.6	1	—	1496*	I	fracture
S4N-1	954	4	0.01	478	—	I	yielding/fracture
S12N-2	954	11.6	0.01	—	796*	I	fracture
S2N-3	25	2	1	—	—	P	no yielding, no fracture
S2N-4	25	2	1	—	—	P	no yielding, no fracture
S4N-4	25	4	1	—	558	P	fracture, no yielding
S6N-3	25	5.5	1	—	532	P	fracture, no yielding
S9N-3	25	9.4	1	—	852	P	fracture, no yielding
S4N-3	25	4	0.01	—	573	P	fracture, no yielding
S6N-2	25	5.5	0.01	—	590	P	fracture, no yielding
S9N-2	25	9.4	0.01	—	805	P	fracture, no yielding
S12N-5	25	11.6	0.01	—	885	P	fracture, no yielding
S12N-6	25	11.6	0.01	—	805	P	fracture, no yielding

C: Compression tests, T: tensile tests, P: plane strain compression tests, B: Brazilian tests (indirect tension tests), and I: indentation tests.

*Results based on pressure/2.8.

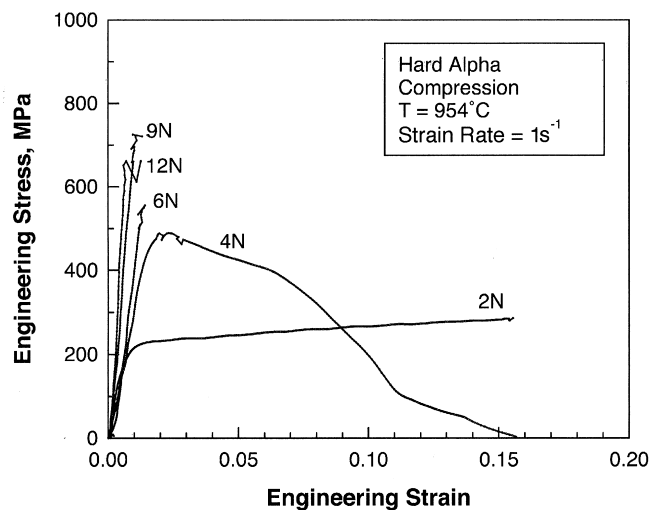


Fig. 4—Compression stress-strain curve of hard-alpha Ti for five different nitrogen contents in weight percent. Tests were conducted at 954 °C under a strain rate of 1 s⁻¹.

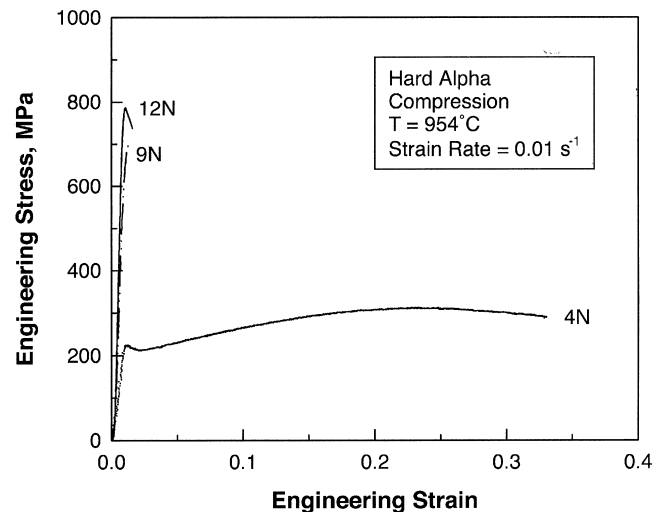


Fig. 5—Compression stress-strain curve of hard-alpha Ti for three different nitrogen contents in weight percent. Tests were conducted at 954 °C under a strain rate of 0.01 s⁻¹.

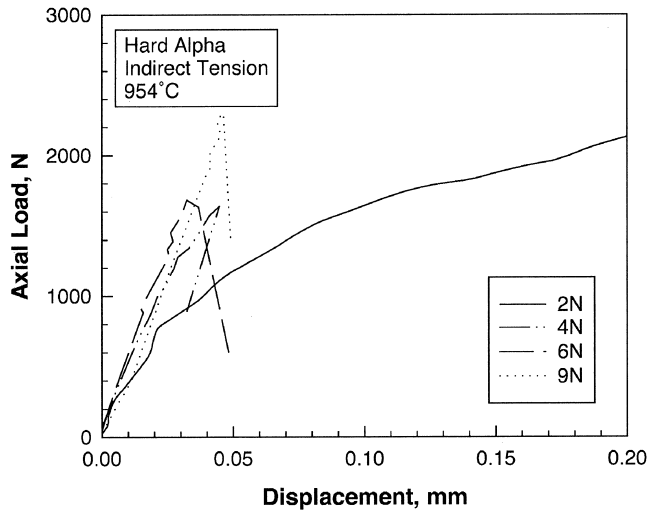


Fig. 6—Load-displacement curves of indirect tension tests of hard-alpha Ti with four different nitrogen contents.

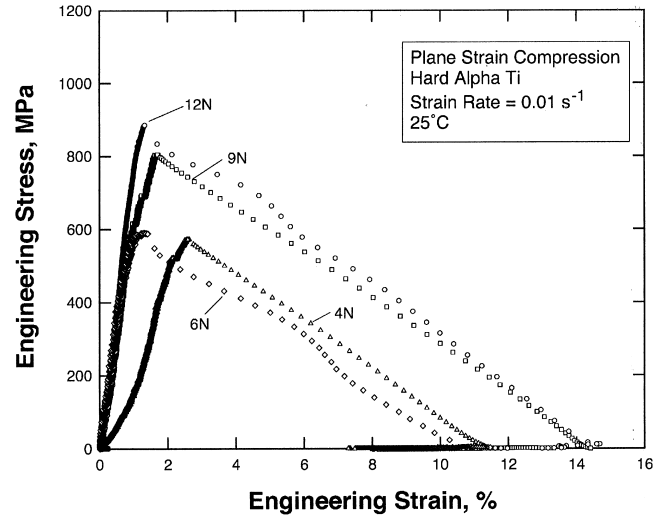


Fig. 8—Comparison of engineering stress-strain curves of hard-alpha Ti with various nitrogen contents tested by plane strain compression at a strain rate of 0.01 s^{-1} .

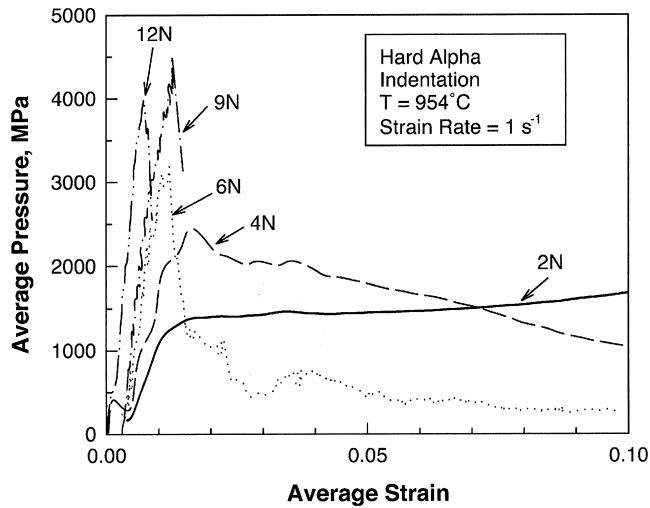


Fig. 7—Experimental results of average pressure vs average strain for indentation of hard-alpha Ti with various nitrogen contents.

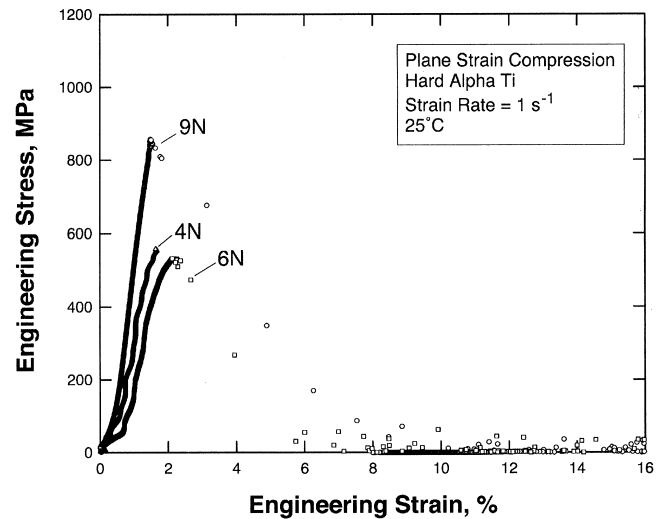


Fig. 9—Comparison of engineering stress-strain curves of hard-alpha Ti with various nitrogen contents tested by plane strain compression at a strain rate of 1 s^{-1} .

plane-strain compression tests in Figures 8 and 9 show that the applied stress in a typical stress-strain curve increases linearly with displacement until a maximum stress is reached. Subsequently, the applied stress decreases almost linearly with increasing displacement. The load drop beyond the peak load was the consequence of the formation of microcracks and fractures by plane-strain compression. Further straining led to comminution of the test specimens and a very low flow stress at large strains. The flow stress is thought to arise from frictional sliding of the comminuted particles.

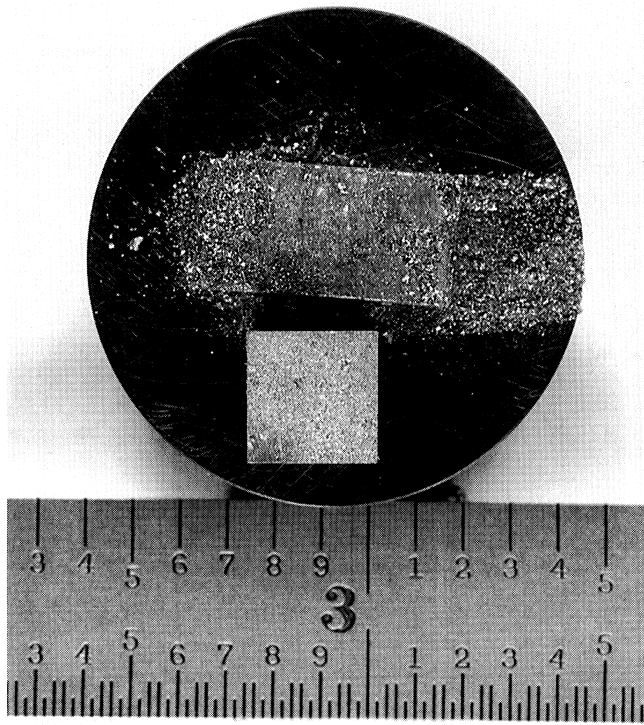
Figure 10 shows a comparison of the test specimens with 4 and 11.6 wt pct N before and after plane-strain compression. Before testing, the 4 wt pct N specimen was in the form of a cube of intact material, but it became a rectangular block of compacted powders after testing. Removing the specimen from the test fixture caused some powders to separate from the block for the 4N material (Figure 10(a)). The 5.5, 9.4, and 11.6 wt pct N test specimens disintegrated into small particles and fine powders when they were removed from the

test fixture, as shown in Figure 10(b) for the 12N material. It appeared that in all cases, the specimens were totally comminuted after deformation but were held together by friction. Removal of the specimens from the test fixture caused some of the comminuted particles to separate from the specimens.

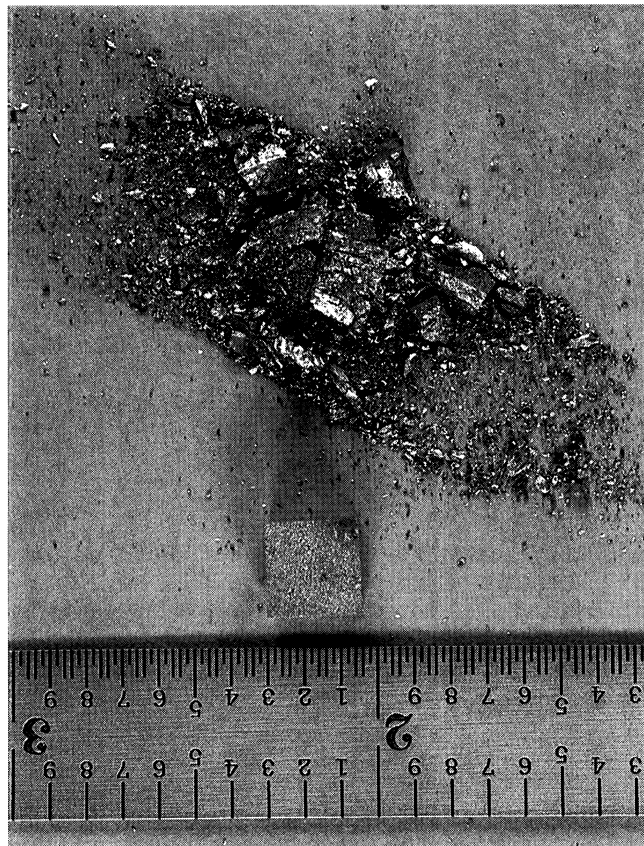
D. Discussion

1. Deformation and fracture characteristics

The deformation and fracture characteristics of hard-alpha test specimens at 954°C or 982°C are summarized in Figures 11(a) through (c) for compression, Brazilian, and indentation test specimens, respectively. In all three cases, the hard-alpha having 2 wt pct N was ductile and deformed without fracture. The hard-alpha Ti having 4 wt pct N exhibited plastic flow followed by fracture, while the hard-alpha Ti

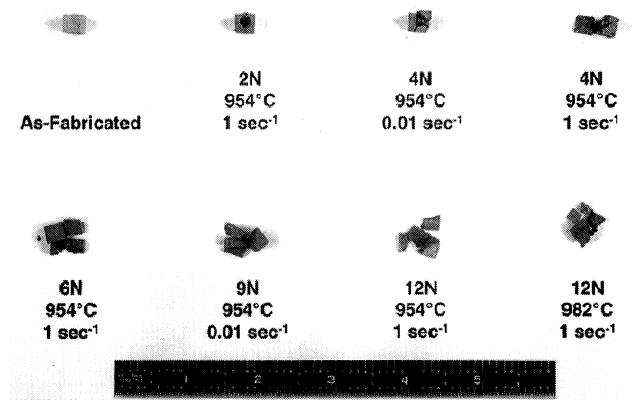


(a)

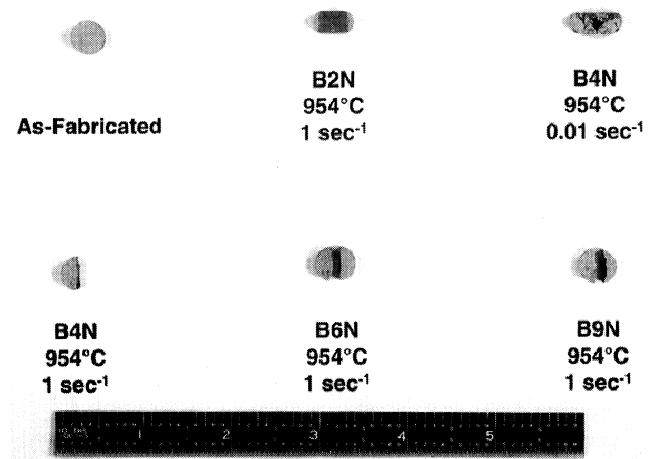


(b)

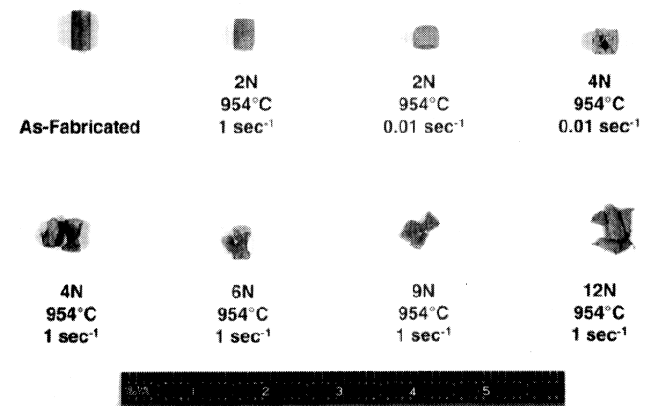
Fig. 10—Comparison of tested and untested plane strain specimens of hard-alpha Ti for two nitrogen contents: (a) 4 pct N and (b) 11.6 pct N.



(a)



(b)

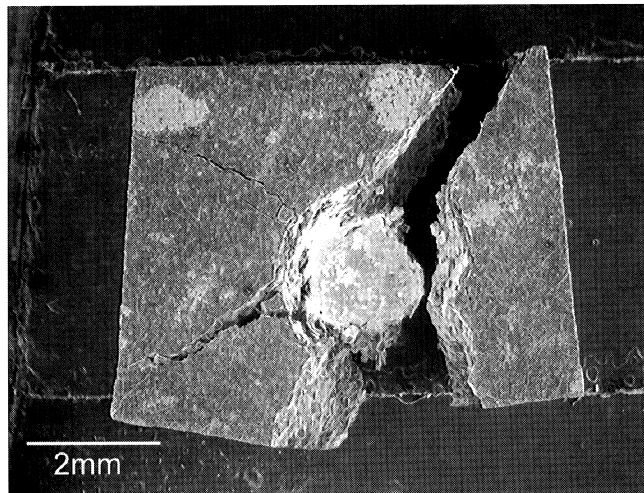


(c)

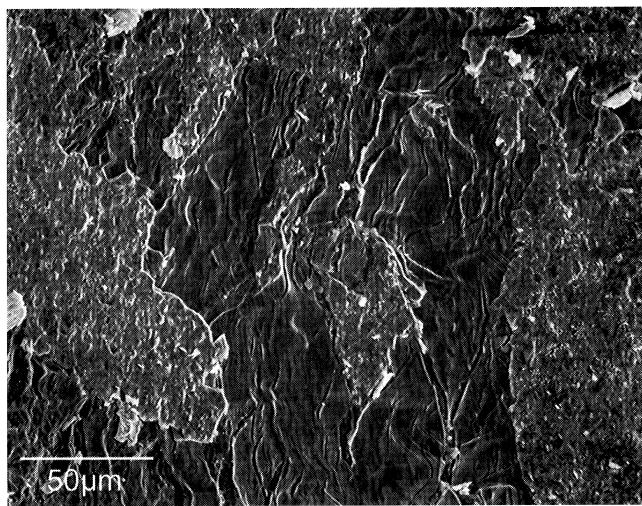
Fig. 11—Geometries of deformed and fractured hard-alpha specimens compared to the as-fabricated condition: (a) compression specimens, (b) indirect tension (Brazilian) specimens, and (c) indentation specimens.

having 5.5 wt pct N or greater fractured into small fragments without showing evidence of plastic flow.

A close-up comparison of the compression specimens with 2 wt pct N (2N) and 4 wt pct N (4N) indicated the absence of apparent cracks or voids in the 2N specimen and the presence of voids and cracks in the 4N material. In the Brazilian tests, the cylindrical disk of the 2 wt pct N material (B2N) was flattened into a more rectangular shape without



(a)



(b)

Fig. 12—(a) Fractured indentations specimen and (b) microcracks at the bottom of the indent for hard-alpha with 4 wt pct N tested at a relatively high strain rate (1 s^{-1}).

causing cracking, while cracks formed in the center of the flattened disk in the 4 wt pct N material (B4N). Thus, there was a large change in the fracture behavior when the nitrogen content increased from 2 to 4 wt pct N. Indentation of the hard-alpha Ti with 4 wt pct N showed strain softening after yielding at both 0.01 and 1 s^{-1} strain rates. Examination of the deformed and fractured specimens of the 4 wt pct N material indicated the presence of several large cracks which fragmented the test specimens. In addition, many microcracks were also observed at the bottom of the indentation, suggesting that the softening effect was probably the consequence of damage or microcracking associated with deformation under the indenter. The fragmented specimens and the microcracks at the bottom of the indent are shown in Figure 12 for the strain rate of 1 s^{-1} . No fractographic analysis was performed to the fractured hard-alpha specimens, but cleavage fracture was expected to be the dominant, if not the only, fracture mode, because of the brittleness of hard-alpha at high nitrogen contents.

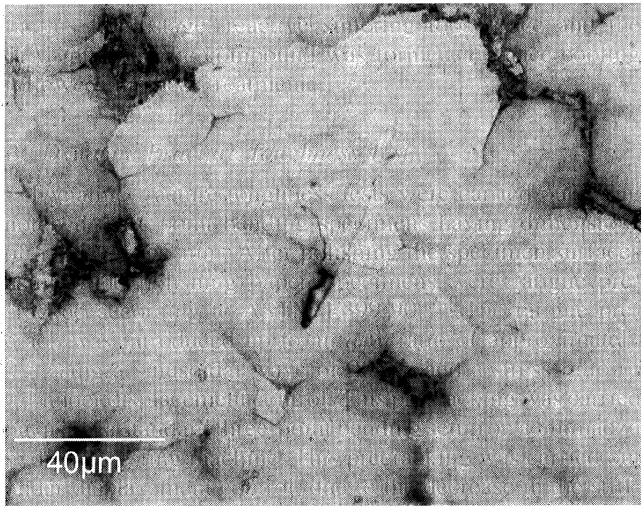
The flow stress of hard-alpha with 2 pct N is dependent on the mean stress (pressure), even though microcracks are

not apparent. The pressure-sensitive flow behavior is contrary to the pressure-insensitive flow behavior exhibited by ductile metals. To better understand this pressure-dependent flow behavior, metallography was performed on sectioned Brazilian, compression, and indentation test specimens. The results show the presence of microcracks and voids in the Brazilian test specimen (Figure 13(a)). Voids are present in the compression specimen as well as in the material below the indent in the indentation specimen (Figures 13(b) and (c)). Compared to the as-received specimens, there were considerably more voids in the deformed specimens. These voids were probably pre-existing porosity or were formed as the result of the reopening of previously closed pores during deformation at a low hydrostatic pressure. Despite the presence of voids, there were no cracks in the compression and indentation specimens (Figure 13(b) and (c)). Thus, the microcracking process appears to occur at low hydrostatic or confining pressures, but is suppressed at higher pressures.

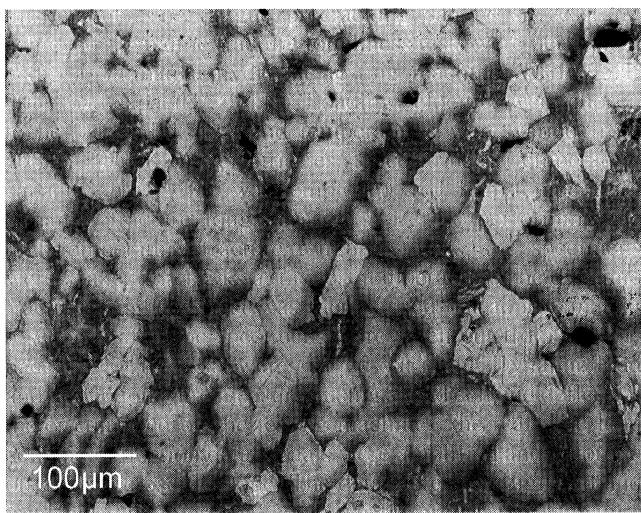
The opening and closure of microcracks by hydrostatic pressure appears to be the source of the pressure-dependent plastic flow behavior observed in the hard alpha. This type of pressure-dependent plastic flow has been observed in rock salt^[17–19] and other brittle solids.^[20–25] The physical and mechanical aspects of this phenomenon are well understood and analyzed.^[17,20–25] The failure mechanism is essentially a pressure-dependent cracking process. When compressing a brittle solid at low hydrostatic or confining pressures, inelastic flow can take place in the form of sliding of boundaries, interfaces, or crack surfaces. A local tensile-stress field exists at the tip of a sliding shear crack or interface. This local tensile stress can cause the formation of a pair of cleavage cracks, referred to as wing cracks, at the tips of the shear crack. These wing cracks are aligned parallel to the axial (loading) direction in uniaxial compression, and their propagation results in a low failure stress and cleavage fracture. The same cracking process operates when a confining or hydrostatic pressure is present. A high confining or hydrostatic pressure, however, can suppress the formation of the wing cracks or prevent them from propagation if they are formed. Because of the suppression of the wing-crack formation by a high confining or hydrostatic pressure, a solid that is brittle in uniaxial tension or compression can deform plastically at high confining or hydrostatic pressures.

For very brittle materials such as hard-alpha containing a high nitrogen content (>5.5 wt pct N) or ceramics such as alumina^[26] and B_4C ,^[27,28] the materials are comminuted during deformation under a high confining pressure. The comminution process appears to be delayed by a high confining or hydrostatic pressure. After the onset of fracture, the “flow” or fracture stress decreases as the number of comminuted particles increases with increasing deformation (Figures 8 and 9). Eventually, a lower-bound flow stress is reached when total comminution has been reached, and the material deforms by frictional sliding along the interfaces of the comminuted particles.

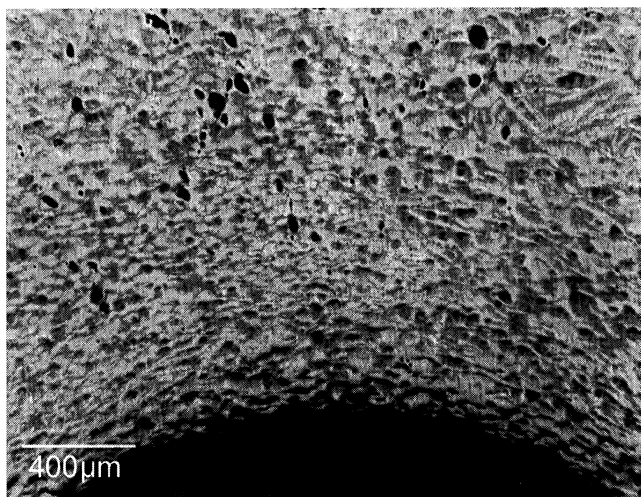
This failure mechanism is consistent with the experimental observation of increasing yield and fracture strengths of hard-alpha with increasing hydrostatic pressure. As shown in Table II, the fracture strength of hard-alpha is about 35 to 49 MPa under indirect tension, but is about 489 to 661 MPa in uniaxial compression. The fracture strength is further



(a)



(b)



(c)

Fig. 13—Damage process in hard-alpha with 2 wt pct N: (a) microcracks in the Brazilian specimen, (b) voids in the compression specimen, and (c) voids in the indentation specimen.

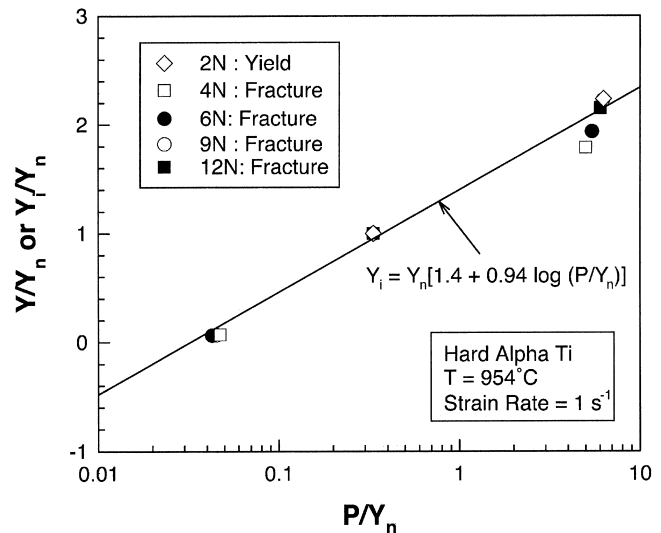


Fig. 14—The flow stress (Y) and fracture stress (Y_i) of hard-alpha increases with increasing pressure, P . All parameters are normalized by the flow or fracture stress for uniaxial compression.

increased to 874 to 1496 MPa under confined deformation by indentation. At lower nitrogen contents (<4 wt pct), where plastic deformation is also present, the yield strength of hard-alpha also increases with increasing hydrostatic pressures.

2. Effects of pressure

The fracture strength (Y_i) determined for a given stress state was normalized by the fracture strength (Y_n) for uniaxial compression. The results are plotted as a function of pressure, normalized by Y_n , in Figure 14. The pressure is calculated as one-third of the sum of the principal stresses, as given by

$$P = \frac{1}{3}(\sigma_{11} + \sigma_{22} + \sigma_{33}) \quad [3]$$

where σ_{11} , σ_{22} , and σ_{33} are the principal stresses. The values of the ratio P/Y_n are 0.045, 1/3, and ≈ 6 for indirection tension, uniaxial compression, and indentation, respectively. The semilog plot in Figure 14 indicates that Y/Y_n increases linearly with $\log (P/Y_n)$. As discussed earlier, the fracture stress increases with hydrostatic pressure because microcracking is suppressed by a high pressure.

3. Effects of nitrogen content

The dependence of the flow and fracture stresses on the nitrogen content of hard-alpha is delineated in Figure 15. Both the flow stress and the fracture stress increase with increasing nitrogen content, but the rates of increase are different, as shown in Figure 15. The flow stress of hard-alpha is lower than the fracture stress at nitrogen contents below 4 wt pct N. The slope dY/dN is higher for the flow stress, and the flow stress exceeds the fracture stress for nitrogen contents higher than 4 wt pct N. As a result, fracture precedes plastic flow when the nitrogen content of hard-alpha is greater than 4 wt pct N.

The addition of N to Ti stabilizes the α -Ti phase and increases the flow stress through interstitial solute strengthening. At high nitrogen contents, a two-phase microstructure of α -Ti and Ti_2N is formed in hard-alphas. At the elevated

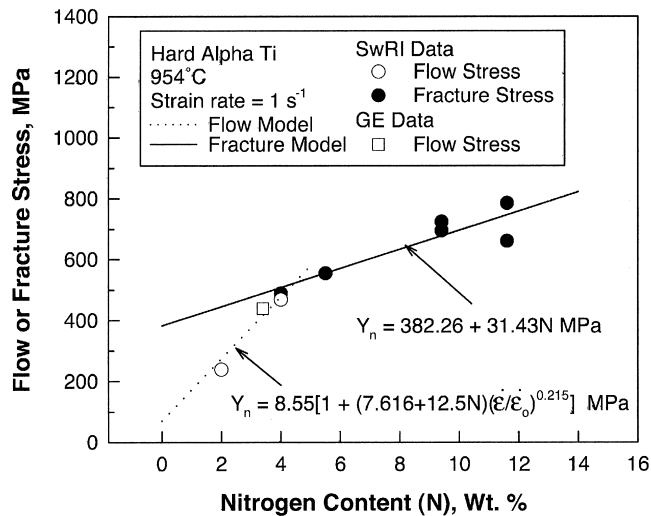


Fig. 15—Flow and fracture stresses of hard- α increase with increasing nitrogen contents at different slopes.

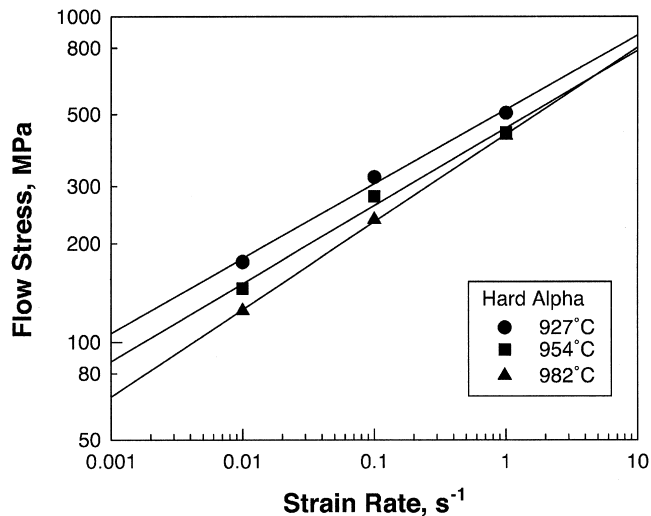


Fig. 16—Flow stress of hard- α with nitrogen content ≤ 4 wt pct increases with increasing strain rate.

test temperatures (927 °C to 982 °C), the hard- α contained a two-phase microstructure of α -Ti and Ti_2N for nitrogen contents >5.5 wt pct N, but contained single-phase α for nitrogen contents <4 wt pct N. Thus, it appears that the effect of N on the flow and fracture behavior of hard- α is the result of the formation of the brittle Ti_2N phase in the microstructure.

4. Effects of strain rate

The effects of strain rate on the flow and fracture stresses of hard α are summarized in Figures 16 and 17, respectively. The result indicates that the flow stress of hard- α increases with increasing strain rate (Figure 16) for materials with less than 4 wt pct N. On the other hand, the experimental data for uniaxial compression and plane-strain compression indicate that the fracture stress of a hard- α specimen having a nitrogen content greater than 5.5 wt pct N is insensitive to the strain rate for the narrow strain rates tested in this study (Figure 17). The fracture stress obtained by the indentation technique shows an apparent rate sensitivity,

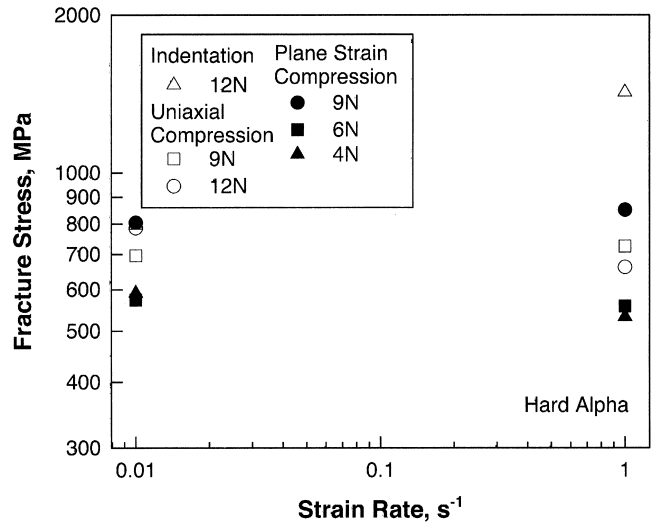


Fig. 17—Fracture strengths of hard- α Ti at two strain rates show little or no rate dependence.

which is not fully understood and could actually be a manifestation of the pressure effect.

5. Effects of temperature

The fracture stress of hard- α with 11.6 wt pct N is relatively insensitive to temperature in the range from 927 °C to 982 °C (Table II). Comparison of the plane-strain fracture stress (845 MPa) at ambient temperature with that for uniaxial compression (812 MPa) suggests that the fracture stress may be independent of temperature from 25 °C to 927 °C. For hard- α with a nitrogen content ≤ 4 wt pct, the flow stress is sensitive to the test temperature and strain rate, as shown in Figure 16.

6. Constitutive relations

As described in detail in a separate publication,^[13] the flow or fracture stress of intact hard- α is given by

$$Y_i = Y_n \left(X + Z \log \left(\frac{P}{\sigma_e} \right) \right) \left(1 + c_0 \epsilon^{c_1} \right) \left(1 + d_0 \left(\frac{\dot{\epsilon}}{\dot{\epsilon}_0} \right)^{d_1} \right) \quad [4]$$

where

Y_i = flow or fracture stress

Y_n = flow or fracture stress under uniaxial compression

P = pressure = $(\sigma_1 + \sigma_2 + \sigma_3)/3$ (compression is positive)

σ_e = von Mises effective stress

$\dot{\epsilon}$ = strain rate

$\dot{\epsilon}_0$ = reference strain rate

ϵ = strain

X and Z = constants related to pressure effects

c_0 and c_1 = constants related to strain-hardening effects

d_0 and d_1 = constants related to strain-rate hardening

and σ_1 , σ_2 , and σ_3 are the principal stresses. In Eq. [4], Y_n is the flow or fracture stress of hard- α under uniaxial compression; this parameter is considered a function of the nitrogen content only. The second term in the right-hand side (RHS) of Eq. [4] represents the increase in the flow or fracture stress with increasing pressure. Strain hardening

and strain-rate hardening are represented by the third and fourth terms on the RHS of Eq. [4], respectively. The parameters X , Z , c_0 , c_1 , d_0 , and d_1 are model constants which are evaluated from experimental data. The reference strain rate ($\dot{\epsilon}_0$) can be taken to be 1 s^{-1} for convenience.

Analyses of the constitutive data of hard-alpha showed that, for fracture, $c_0 = d_0 = 0$, because of the lack of strain and strain-rate hardening. The values of X and Z are 1.4 and 0.94, respectively, as shown in Figure 14. The fracture stress at uniaxial compression shows a linear correlation with the nitrogen content, which can be represented by

$$Y_n = \gamma_0 + \gamma_1 N \quad [5]$$

where γ_0 and γ_1 are correlation coefficients. Linear regression of the experimental data (Figure 15) allows determination of the values of γ_0 and γ_1 , leading to $\gamma_0 = 382.3 \text{ MPa}$ and $\gamma_1 = 31.43 \text{ MPa/wt pct N}$, as shown in Figure 15.

The flow stress is a general function of strain and strain rate, as described by

$$Y_n = Y_0 (1 + c_0 \epsilon^{c_1}) \left(1 + d_0 \left(\frac{\dot{\epsilon}}{\dot{\epsilon}_0} \right)^{d_1} \right) \quad [6]$$

where Y_0 , c_0 , c_1 , d_0 , and d_1 are constants, ϵ is the strain, $\dot{\epsilon}_0$ is the reference strain rate, and $\dot{\epsilon}$ is the strain rate. Analysis of the flow-stress data led to $c_0 = 0$ because of the lack of strain hardening. The strain-rate exponent d_1 has a value of 0.215. The value of d_0 is a linear function of nitrogen, as given by

$$d_0 = 7.616 + 12.5 N \quad [7]$$

and $Y_0 = 8.55 \text{ MPa}$, as shown in Figure 15.

III. CONCLUSIONS

The constitutive properties of hard-alpha Ti have been characterized as a function of stress state, nitrogen content, strain rate, and temperature. The conclusions reached in this study are as follows.

1. At a typical forging temperature of 954 °C, hard-alpha Ti with nitrogen contents less than 4 wt pct is ductile and can be plastically deformed in compression or under indirect tension. With nitrogen contents at or greater than 5.5 wt pct, hard-alpha Ti is brittle and exhibits elastic fracture in compression, indirect tension, and indentation.
2. The fracture stress of hard-alpha is considerably lower in tension (35 to 70 MPa) than in compression (489 to 725 MPa).
3. The flow and fracture stresses of hard-alpha Ti increase with increasing pressure, because of suppression of microcrack formation at high pressures.
4. The flow stress of hard-alpha Ti increases with increasing strain rate, but the fracture stress is insensitive to the strain rate.
5. The fracture stress of hard-alpha Ti is relatively insensitive to temperature in the range of 25 °C to 980 °C.
6. The flow and fracture stresses of hard-alpha Ti increases with increasing nitrogen content.

ACKNOWLEDGMENTS

This work was supported by the Federal Aviation Administration, Department of Transportation, through Grant No.

95-G-041, Dr. Bruce Fenton and Dr. Joe Wilson, Program Managers. Technical assistance provided by Mr. F. Campbell in mechanical testing and Mr. B. Chapa in metallography is acknowledged. The clerical assistance by Ms. L. Salas in preparing the manuscript is appreciated.

REFERENCES

1. F.W. Wood: "Elimination of Low-Density Inclusions in Titanium Alloy Ingots," AFML-TR-69-47, Air Force Materials Laboratory, Wright-Patterson Air Force Base, Dayton, OH, 1969.
2. Titanium Rotating Components Review Team Report, Federal Aviation Administration, Washington, DC, Dec. 14, 1990.
3. *Damage Tolerance Concepts for Critical Engine Components*, AGARD Conf. Proc. No. 393, Advisory Group for Aerospace Research and Development, NATO, Neuilly-Sur-Seine, France, 1985.
4. J.C. Newmar, Jr: Contribution from NASA Langley Research Center on the AGARD Engine Disc Programme, private correspondence, NASA Langley Research Center, Langley, VA, 1994.
5. P.G. Roth: "Probabilistic Rotor Design System (PRDS) Phase I," AFWAL Report WL-TR-92-2011, AFWAL, Dayton, OH, May 1992.
6. J.D. Adamson, E.P. Fox, and J.E. Malone: Probabilistic Design System—Phase I and II Interim Report, Contract No. F33615-92-C-2219, Pratt & Whitney, West Palm Beach, FL, Dec. 1995.
7. D. Sundararaman, V. Seetharaman, and V.S. Raghunathan: in *Titanium '80*, H. Kimura and O. Izumi, eds., TMS-AIME, Warrendale, PA, 1980, pp. 1521-32.
8. C.E. Shamblen, G.B. Hunter, W.H. Buttrill, and E.L. Raymond: "Manufacturing Technology for Premium Quality Titanium Alloys for Gas Turbine Engine Rotating Components, Phase I—Vol. 1: Technical Program," WL-TR-92-8078, Wright-Patterson Air Force Base, Dayton, OH, 1993, pp. 135-54.
9. M.F.X. Gigliotti, R.S. Gilmore, and L.C. Perocchi: *Metall. Mater. Trans. A*, 1994, vol. 25A, pp. 2321-29.
10. L.J.H. Brasche, F. Margetan, and R.B. Thompson: *Review of Progress in Quantitative Nondestructive Evaluation*, Plenum Press, New York, NY, 1992, pp. 1733-38.
11. M. Gigliotti: GE CR&D Internal Report, GE CR&D Center, Schenectady, NY, 1991.
12. H.A. Wriedt and J.L. Murray: in *Binary Alloy Phase Diagrams*, 2nd ed., T.B. Massalski, ed., ASM, Materials Park, OH, 1990, vol. 3, p. 2607.
13. K.S. Chan: Southwest Research Institute, San Antonio, TX, unpublished research, 1999.
14. M.C. Shaw, P.M. Braiden, and G.J. DeSalvo: *J. Eng. Industry, Trans. ASME* 1975, Ser. B, vol. 97 (1), pp. 77-87.
15. D. Tabor: *The Hardness of Metals*, Oxford University Press, New York, NY, 1951.
16. G.E. Dieter, Jr.: *Mechanical Metallurgy*, McGraw-Hill, New York, NY, 1961, pp. 286-89.
17. K.S. Chan, D.E. Munson, S.R. Bodner, and A.F. Fossum: *Acta Mater.*, 1996, vol. 44, pp. 3553-65.
18. K.S. Chan, N.S. Brodsky, A.F. Fossum, D.E. Munson, and S.R. Bodner: *J. Eng. Mater. Technol.*, 1997, vol. 119, pp. 393-400.
19. K.S. Chan, D.E. Munson, and S.R. Bodner: in *Fracture of Rock*, M.H. Aliabadi, ed., WIT Press, Boston, MA, 1999, pp. 331-79.
20. W.F. Brace, B.W. Paulding, Jr., and C. Sholz: *J. Geophys. Res.*, 1966, vol. 71, pp. 3939-53.
21. S. Nemat-Nasser and H. Horii: *J. Geophys. Res.*, 1982, vol. 87, pp. 6805-21.
22. H. Horii and S. Nemat-Nasser: *J. Geophys. Res.*, 1985, vol. 90, pp. 3105-25.
23. C.G. Sammis and M.F. Ashby: *Acta Metall. Mater.*, 1986, vol. 34, pp. 511-26.
24. M.F. Ashby and S.D. Hallam: *Acta Metall. Mater.*, 1986, vol. 34, pp. 497-510.
25. S.D. Hallam and M.F. Ashby: in *Deformation Processes in Minerals, Ceramics, and Rocks*. D.J. Barber and P.G. Meredith, eds., Routledge Chapman & Hall, New York, NY, 1990, pp. 84-108.
26. J. Lankford, C.E. Anderson, Jr., A.J. Nagy, J.D. Walker, A.E. Nichollis, and R.A. Page: *J. Mater. Sci.*, 1998, vol. 33, pp. 1619-25.
27. L.W. Meyer and I. Faber: *J. Phys. IV*, 1997, vol. 7, pp. C3-565-C3-570.
28. G.R. Johnson and T.J. Holmquist: *J. Appl. Phys.*, 1999, vol. 85 pp. 8060-73.